INTERNATIONAL JOURNAL OF HYDROGEN ENERGY 42 (2017) 24978–24988

Available online at www.sciencedirect.com

ScienceDirect

journal homepage: www.elsevier.com/locate/he

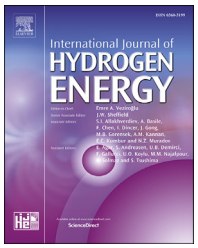

A highly scalable spray coating technique for electrode infiltration: Barium carbonate infiltrated $La_{0.6}Sr_{0.4}Co_{0.2}Fe_{0.8}O_{3-\delta}$ perovskite structured electrocatalyst with demonstrated long term durability

Tao Hong [a], *Shiwoo Lee* [b,e], *Paul Ohodnicki* [c,d], *Kyle Brinkman* [a,*]

[a] *Department of Materials Science and Engineering, Clemson University, Clemson, SC 29634, USA*
[b] *United States Department of Energy, National Energy Technology Laboratory, Morgantown, WV 26507, USA*
[c] *United States Department of Energy, National Energy Technology Laboratory, Pittsburgh, PA 15236, USA*
[d] *Materials Science and Engineering Department, Carnegie Mellon University, Pittsburgh, PA 15213, USA*
[e] *AECOM, Morgantown, WV 26507, USA*

ARTICLE INFO

Article history:
Received 1 May 2017
Received in revised form
13 August 2017
Accepted 14 August 2017
Available online 8 September 2017

Keywords:
Spray coating
Oxygen reduction reaction
Barium carbonate
Cathode reaction
Solid oxide fuel cells

ABSTRACT

This work demonstrated a highly scalable spray coating process for cathode infiltration with excellent long-term stability for the oxygen reduction reaction. Barium carbonate ($BaCO_3$) nanoparticles have previously demonstrated excellent catalytic activity for the oxygen reduction reaction and were chosen as a model system to be applied by spray coating onto $La_{0.6}Sr_{0.4}Co_{0.2}Fe_{0.8}O_{3-\delta}$ (LSCF) and LSCF-SDC ($Sm_{0.2}Ce_{0.8}O_{2-\delta}$) cathode materials. In this work, barium acetate solutions were modified by a surfactant to lower the surface tension and decrease the contact angle on LSCF which is a benefit for the infiltration process. In the LSCF electrode, $BaCO_3$ nano-particles exhibited significant interfacial contact with LSCF particles by the spray coating technique. As a result, the polarization resistance of $BaCO_3$ infiltrated LSCF was reduced from 2.5 to 1.2 Ωcm^2 at 700 °C. In addition, commercial full cell SOFCs with $BaCO_3$ infiltrated LSCF-SDC cathodes also demonstrated higher performance due to the reduced cathode resistance. At 750 °C, the electrode overpotential of the $BaCO_3$ infiltrated cell was much lower than that of baseline cell during long term testing (500 h). The polarization resistance of the $BaCO_3$ infiltrated LSCF-SDC electrode only increased by 1.6% after 500 h.

Introduction

Solid oxide fuel cells (SOFCs) enable highly efficient electricity generation from a wide variety of chemical fuels [1–6]. For a given electrolyte material and thickness, the performance is largely determined by the electrode process, especially the cathode due to the high activation energy associated with the oxygen reduction reaction (ORR) [7–9]. The nano-scale and nano-structured electrodes achieved by

* *Corresponding author.*
E-mail address: ksbrink@clemson.edu (K. Brinkman).
http://dx.doi.org/10.1016/j.ijhydene.2017.08.091

the impregnation/infiltration method have attracted increased attention due to their high electrochemical activities resulting from the enlarged surface area for catalytic reaction and enhanced three-phase boundaries (TPBs), where the electrode catalyst, electrolyte and gas phases intersect [10–13].

The most distinctive advantage of the nano-structured approach is the flexibility for the selection and combination of highly active catalytic materials with structurally stable mixed ionic and electronic conducting (MIEC) scaffolds that meet the stringent requirements of SOFCs cathodes [14–19]. In order to further improve the performance of cathode materials, active electrocatalysts may be applied to the backbone surface [20,21]. For example, $La_{0.6}Sr_{0.4}Co_{0.2}Fe_{0.8}O_{3-\delta}$ (LSCF) is an excellent MIEC materials which shows great performance at intermediate temperature, but still suffers from low surface activity for the ORR at lower temperature and inadequate long-term durability [22–24]. Surface modification through infiltration is an effective approach to enhance cathode functionality while retaining the advantages of the constituent cathode material. There has been a wide range of infiltration phases that have been applied to the LSCF cathode backbone. For example, $La_{0.6}Sr_{0.4}Co_{0.2}Fe_{0.8}O_{3-\delta}$ (LSCF) electrode infiltrated with 1.5 $mgcm^{-2}$ $Gd_{0.1}Ce_{0.9}O_{2-\delta}$, exhibited significant interfacial resistance reduction from 0.22 to 0.06 Ωcm^2 at 750 °C [25]. Also, the addition of $La_{0.85}Sr_{0.15}MnO_{3-\delta}$ (LSM) as an infiltration material resulted in improved performance over long term durability testing with a constant voltage of 0.8 V at 750 °C for 500 h [26]. $BaCO_3$ is a non-electronic/ionic conductor that has demonstrated excellent ORR catalytic activity when infiltrated into a number of common SOFC cathode materials [27–29]. $SrCO_3$, similar to $BaCO_3$, has also been reported to improve cathode performance, however the magnitude of the enhancement factor is much lower than that of $BaCO_3$ [30]. While other materials such as CoO_x and CaO [31–34] have also been reported to improve the cathode performance, their enhancements were primarily attributed to physical effects including enhanced interfacial bonding and contact between infiltration phase and the electrode. Finally, not all oxides/carbonates appear to be good candidates for infiltration. Recent reports utilizing Al_2O_3 have shown a degradation of performance when deposited into the cathode backbone [35].

Infiltration methods like electro deposition and electro less deposition have also been used to accelerate the infiltration process [18,36]. However, the electro deposition and electro less deposition require the porous scaffold to be conductive. Compared with conventional infiltrating, spray coating is a more effective and convenient method to disperse the solution into the electrode scaffold [37]. Distribution of infiltrated nanoparticles also depends on the wetting properties between the metal salt solution and the porous scaffold. Adding surfactants or complexing agents is beneficial for the uniform distribution and phase formation of infiltrated nanoparticles. For example, the addition of urea and polymeric dispersant can facilitate the formation of a perovskite phase such as $Sm_{0.6}Sr_{0.4}CoO_3$ and LSM at low temperatures [38,39], presumably due to the complexing effect of the additives.

Despite the additional chemical complexity of tailored solutions associated with the infiltration method, nanoscale engineering of electrode structures via infiltration is shown to be a highly effective way to produce highly active and advanced electrode structures for SOFCs. Modeling simulations incorporating the microstructural, electrochemical and catalytic aspects of the infiltrated nanoparticle have provided an additional assessment of the promise of nano-structured electrodes [40–44].

In this work, we extend our investigations by using spray coating and surfactant modified barium acetate solution to investigate the ORR activity of $BaCO_3$ nanoparticles in SOFC cathode. The results indicate significantly enhanced performance of the spray coated materials as compared to conventional infiltration methods. In addition, commercial full cell SOFCs with $BaCO_3$ infiltrated LSCF-$Sm_{0.2}Ce_{0.8}O_{2-\delta}$ (SDC) cathodes also demonstrated higher performance due to the reduced cathode resistance indicating stable operation with limited degradation over a 500 h long term test.

Experiment

Powder preparation

LSCF ($La_{0.6}Sr_{0.4}Co_{0.2}Fe_{0.8}O_{3-\delta}$) powder was prepared by an EDTA-citric acid combustion method [23]. Stoichiometric amounts of the precursors $La(NO_3)_3$, $Sr(NO_3)_2$, $Co(NO_3)_3$ and $Fe(NO_3)_3$ (99.5% Sinopharm Chemical Reagent Co. Ltd) were dissolved in distilled water. Citric acid and EDTA were used at the molar ratio of metal cation: citric acid: EDTA = 1: 1: 1 to assist the combustion process. The precursor solution was subsequently heated on a hot plate until self-combustion occurred and then the resulting ashes were calcined at 800 °C for 2 h to remove possible organic residues and to form the desired perovskite structure.

Symmetric cells with two identical LSCF cathodes were fabricated on both sides of the $Gd_{0.2}Ce_{0.8}O_{2-\delta}$ (GDC) electrolytes in order to evaluate the interfacial polarization resistance. Dense cylindrical GDC pellets were prepared by uniaxially pressing the GDC powders (Fuelcell Company Co. Ltd) followed by sintering at 1450 °C for 5 h. The LSCF slurries were prepared by mixing the LSCF powders with an organic binder. The as-prepared slurry was printed onto both sides of the GDC pellets. After drying under an infrared lamp, the structure was heated at 1000 °C for 2 h to form the symmetrical cells.

Appropriate amounts of barium acetate, $Ba(Ac)_2$ (Alfa Aesar 99%, Co. Ltd) were dissolved in water to form 0.3 $molL^{-1}$ solution. Triton™ X-100 (Sigma-Aldrich) was used as surfactant. The conventional infiltration was carried out by placing a drop of solution on the top of the LSCF electrode structure, letting the solution soak into the porous backbone, followed by drying, and firing the sample at 800 °C in air for 1 h to form the $BaCO_3$ nanoparticle catalyst. The spray coating technique utilized an ultrasonic sprayer (Sono-Tek®) with an operating frequency of 120 kHz to infiltrate the cathode with an atomized solution.

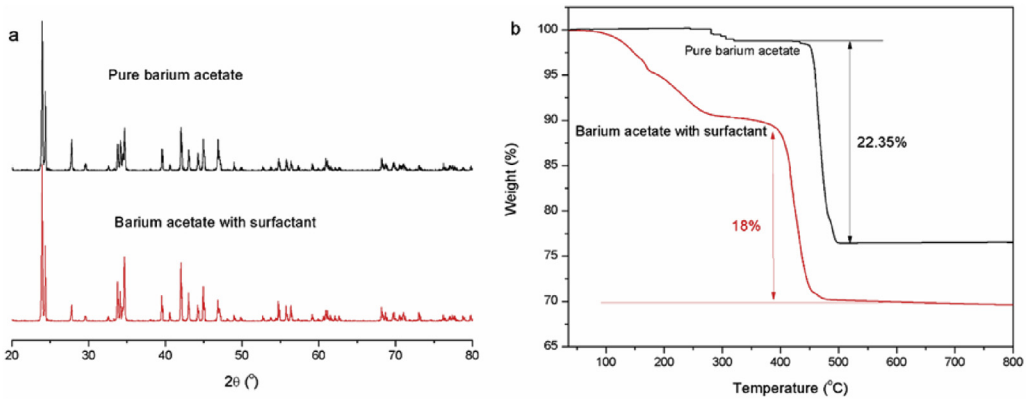

Fig. 1 – (a) XRD pattern for $BaCO_3$ deprived from decomposition of pure $Ba(Ac)_2$ and $Ba(Ac)_2$ with surfactant and (b) Thermogravimetric curve for $Ba(Ac)_2$. (The measurement is conducted in air atmosphere with a flow rate of 75 ml min^{-1}.)

Commercial anode-supported full cells (MSRI, Salt Lake City, UT) consisting of an LSCF-SDC (20 mol% Samaria doped Ceria) cathode were also used as backbone for $BaCO_3$ infiltration. The commercial full cell architecture was as follows: 10 μm-thick YSZ electrolyte is supported by a 750 μm-thick Ni-YSZ anode and cathode with a 2 cm^2 active area. A functional layer of LSCF-SDC (10 μm thick), situated between a dense SDC buffer layer on the electrolyte and a LSCF current collecting layer (50 μm thick) are also utilized.

Characterization of phase composition and microstructure of cathodes

X-ray diffraction (Rigaku TTR-III) analysis was used to examine the phase purity of $BaCO_3$ powders. The microstructure and morphology of the $BaCO_3$ infiltrated LSCF cathodes were examined using a scanning electron microscope (SEM, Hitachi S-4800). The nano-structure of LSCF and $BaCO_3$, energy dispersive spectroscopy (EDS) and selected area electron diffraction (SAED) result were

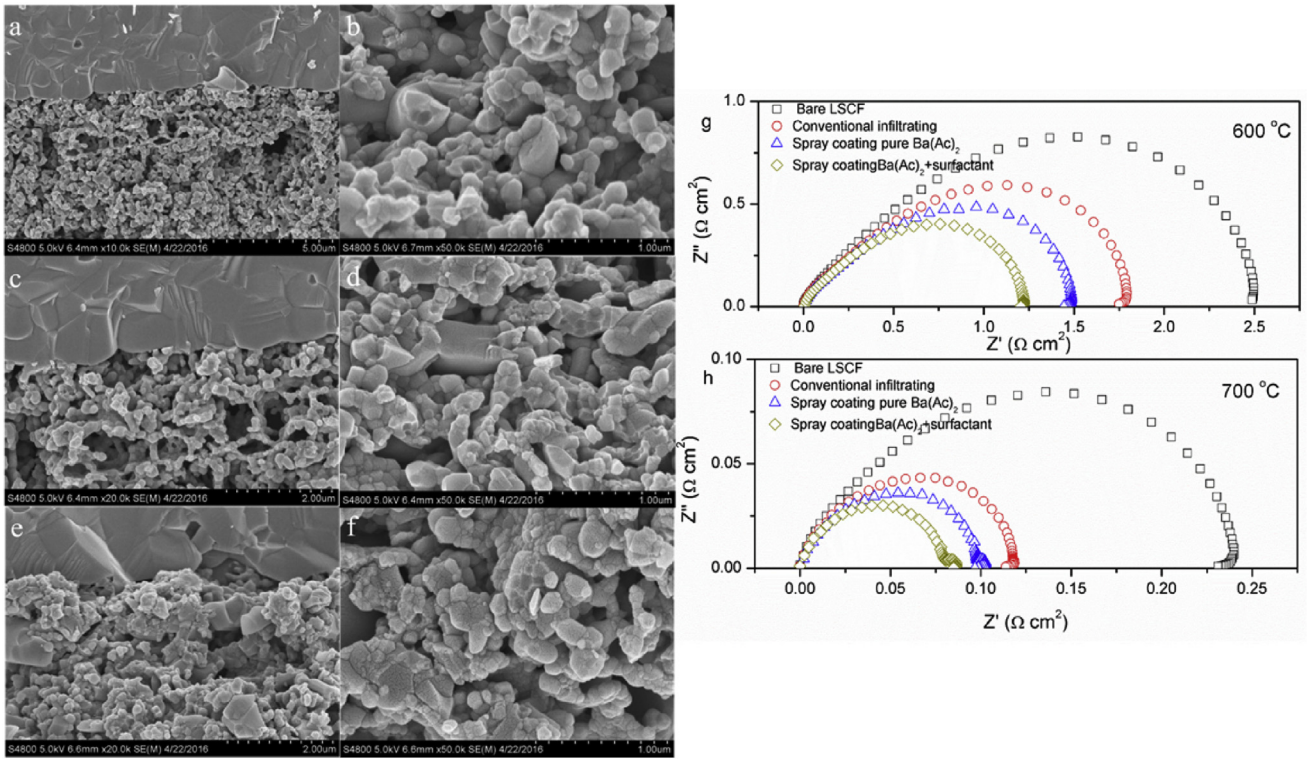

Fig. 2 – The cross-section SEM images for LSCF electrode with different infiltrating method: (a–b) conventional infiltrating with pure barium acetate solution, (c–d) spray-coating with pure barium acetate solution and (e–f) spray-coating barium acetate solution with surfactant. And the impedance spectra at g) 600 °C and h) 700 °C for symmetrical cell consisting of LSCF electrodes on GDC electrolyte as a function of infiltration conditions.

investigated by transition electron microscope (TEM, Hitachi H-9500) after scraping material from the infiltrated cathode onto TEM grids.

Electrochemical measurement

The electrochemical performance of cathodes was measured using the symmetric cells configuration with Ag as the current collector. Impedance spectra were acquired using a Solartron 1260 electrochemical workstation with an AC amplitude of 10 mV in the frequency range from 1 M Hz to 0.1 Hz. AC impedance plots were fitted using Zview software according to the equivalent circuit with a standard deviation below 5%.

The commercial fuel cells were tested at the multi-cell testing system installed at the NETL (Morgantown, WV) under wet H_2 for anode and dry air for cathode at 750 °C for ~ 500 h. The system can test up to 12 cells in a parallel cell array connected to a common fuel and air manifold. Impedance spectra were measured at various polarization conditions in the galvanostatic mode with a frequency range of 0.05–0.1 MHz and 10–50 mV perturbation using a frequency response analyzer (Solartron 1455A) and a potentiostat (Solartron 1470E). An electronic load (Agilent N3301A) was used to apply constant current of 0.25 Acm^{-2} to the cells during the tests.

Results and discussion

Thermal decomposition of barium acetate

Fig. 1a shows the $BaCO_3$ XRD patterns derived from decompose of barium acetate and barium acetate with surfactant at 800 °C. Both of the $BaCO_3$ XRD patterns display the orthorhombic structure (Pmcn 62), suggesting that the surfactant doesn't change the final decomposition product of $Ba(Ac)_2$. The decomposition processes during heating in air of $Ba(Ac)_2$ with and without surfactant was investigated using thermogravimetric measurements as displayed in Fig. 1b. Pure $Ba(Ac)_2$ without surfactant displayed 1.368% weight loss in the range from 280 to 300 °C, possibly due to the loss of adsorbed water. At 400 °C, a significant weight

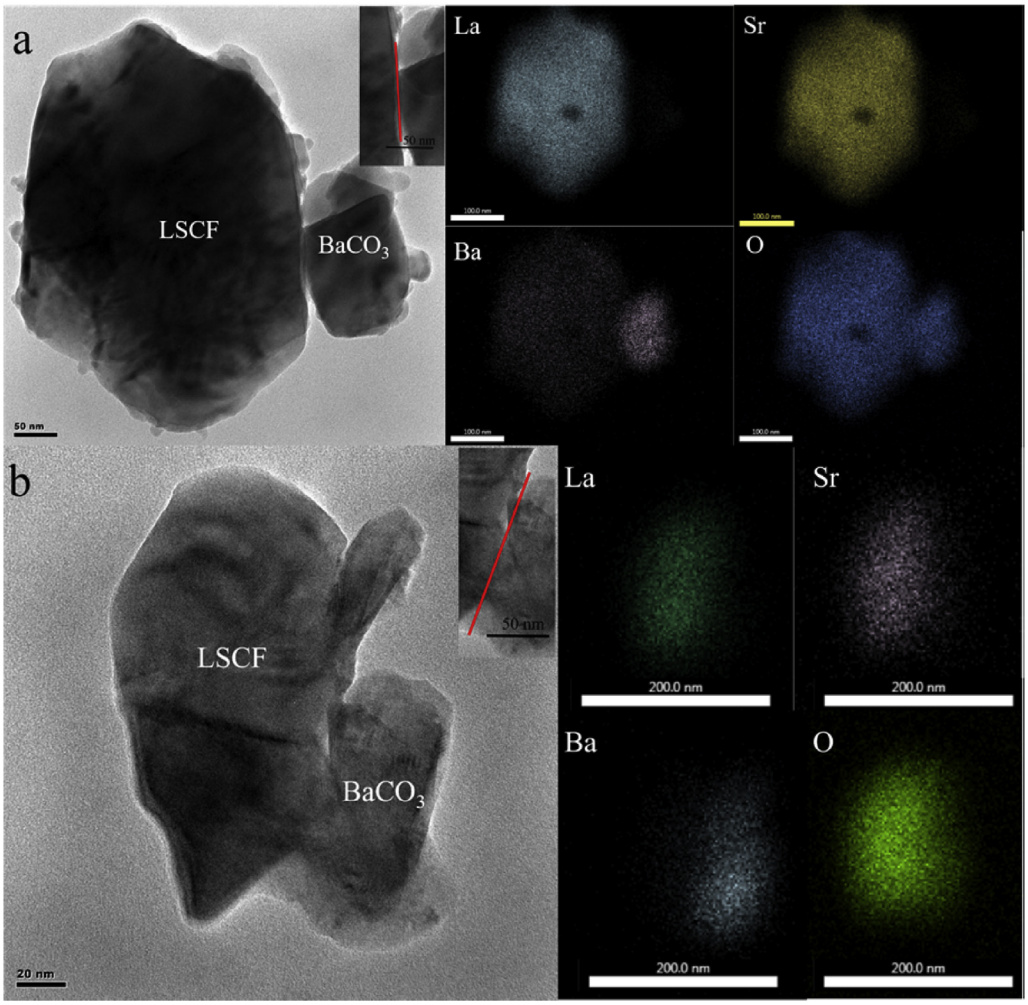

Fig. 3 – TEM images for LSCF and $BaCO_3$ particles derived from (a) pure $Ba(Ac)_2$ solution and (b) modified $Ba(Ac)_2$ solution. The energy dispersive spectrometer (EDS)-mapping images of La, Sr, Ba and O element are also presented. The boundary length is also labeled in the inset images of a and b.

loss event 22.35% was experienced due to the formation of $BaCO_3$. The observed relative weight loss at 400 °C is 22.35%/(100%–1.368%) = 22.66%, which is very close to the theoretical prediction of 22.75% for the decomposition reaction of $Ba(Ac)_2$ = $BaCO_3$ +CO_2+H_2O. $Ba(Ac)_2$ with surfactant Triton™ X-100 has a critical micelle concentration (CMC) of 0.23 mM. The high viscosity of the surfactant made it difficult to precisely control the amount added, however the additions exceeded the CMC. The starting decomposition temperature in air of $Ba(Ac)_2$ with surfactant was 400 °C which is 50 °C lower than pure $Ba(Ac)_2$. This result indicated that the added surfactant impacted the solution chemistry resulting in weight loss associated with $BaCO_3$ formation occurring at a lower temperature as compared to pure $Ba(Ac)_2$ solutions.

The electrochemical performance of LSFC electrodes with different infiltration methods

Typical cross-sectional views of a LSCF electrode supported on a dense GDC electrolyte are shown in Fig. 2. As seen in Fig. 2a the LSCF layer is porous with a grain size in the range of 0.2–0.3 μm. In the conventional infiltration process, $Ba(Ac)_2$ solution was deposited onto bare LSCF, dried and heated to form $BaCO_3$ as seen in Fig. 2a–b. Images of the deposition process following spray coating with pure $Ba(Ac)_2$ solution are shown in Fig. 2c–d indicating the solution penetrated the porous electrode to a greater extent, possibly due to atomization of a controlled amount of solution droplets. In further experiments, the addition of surfactant was found to modify the solution properties. For example, the surface tension of a pure solution was 75.3×10^{-3} (N/m) as compared to 32.8×10^{-3} (N/m) for the modified solution. In addition, the contact angle of the solution on the LSCF surface was reduced from 62.7° to 33.6° which means the solution could cover the LSCF backbone easier and more uniform during the spray coating process. Fig. 2e–f displays images of modified solution spray coating indicating enhanced $BaCO_3$ formation in the area close to GDC electrolyte.

Fig. 2g–h shows the typical impedance spectra measured at 600 and 700 °C for symmetrical cells with LSCF electrodes supported on a GDC electrolyte. For the bare LSCF electrode, the ASR at 600 °C was 2.5 Ωcm^2, which is similar to a number of reported values for the LSCF/GDC system [25,45,46]. The sample prepared by conventional infiltration exhibited a decreased value of 1.8 Ωcm^2. Samples prepared by the spray coating method also demonstrated reduction in polarization resistance. The pure $Ba(Ac)_2$ solution had a value of 1.5 Ωcm^2, while the surfactant modified $Ba(Ac)_2$ solution showed further reduction down to a value of 1.2 Ωcm^2.

Fig. 3 displays the results of TEM-EDS analysis for the LSCF and $BaCO_3$ particles formed by the spray coating technique. For the sample made from pure $Ba(Ac)_2$, the $BaCO_3$ particle size was approximately 100 nm. EDS mapping images of La, Sr and Ba (mapping images of Fe and Co element are not shown due to TEM chamber background interference with the Fe and Co signals) confirm that the lager particle is LSCF and smaller particle is $BaCO_3$. For the sample spray coated with a modified $Ba(Ac)_2$ solution, EDS mapping also indicate the smaller particle (80 nm) is $BaCO_3$. The boundary length between LSCF and $BaCO_3$ is also labeled in the inset images of Fig. 3. The boundary length of the modified solution was approximately 150 nm, which was larger than the un-modified solution boundary length of 110 nm. This suggests that interfacial contact between the LSCF and $BaCO_3$ particles was enhanced with the solution modified $Ba(Ac)_2$ spray coated process and is consistent with the previously mentioned contact angle results indicating that modified $Ba(Ac)_2$ solution possessed a smaller contact angle on LSCF, resulting in enhanced interfacial bonding after $Ba(Ac)_2$ decomposition to $BaCO_3$.

Fig. 4a summarizes the effects of $BaCO_3$ loading (samples prepared by spray coating from a modified solution) on the polarization resistance, which was determined from the AC impedance spectra. The resistance decreased substantially after the porous LSCF electrode was infiltrated with $BaCO_3$ nanoparticles. For example, at 700 °C, the bare LSCF electrode displayed an ASR of 0.25 Ωcm^2. This resistance decreased to 0.15 Ωcm^2 with a $BaCO_3$ loading of 0.67 mgcm^{-2} (4 wt% $BaCO_3$),

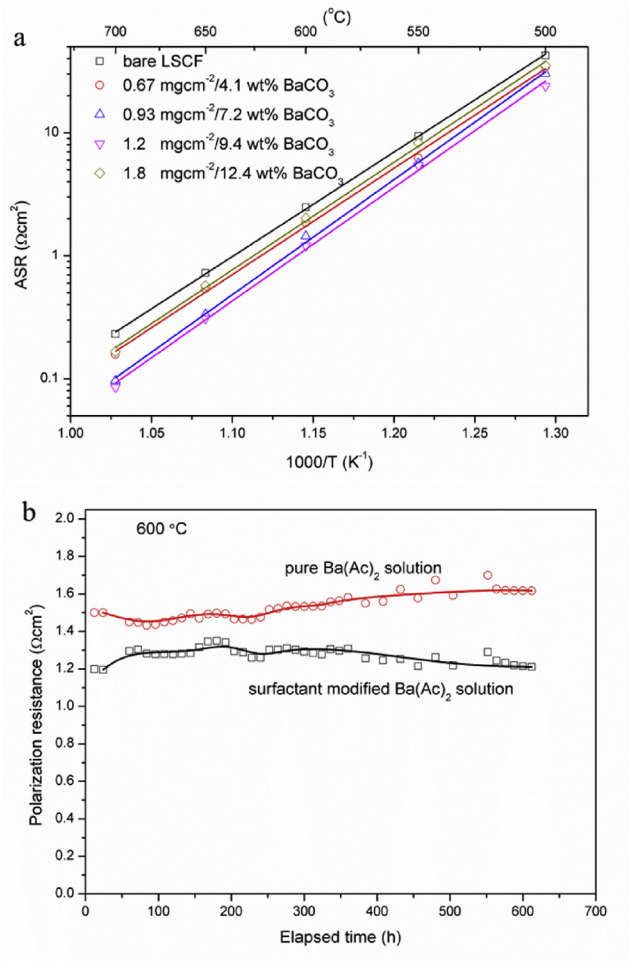

Fig. 4 – (a) The Arrhenius relationship between area-specific interfacial polarization resistance (ASR) and temperature for LSCF electrodes spray coated with different loadings of $BaCO_3$. And (b) the polarization resistance evolution of the LSCF electrode spray coated with pure and surfactant modified $Ba(Ac)_2$ solution after extended testing at 600 °C for 600 h.

and further decreased to 0.09 and 0.08 Ωcm^2 at $BaCO_3$ loadings of 0.93 (7.2 wt% $BaCO_3$), and 1.2 $mgcm^{-2}$ (9.4 wt% $BaCO_3$), respectively. However, further increase in the loading resulted in a slight increase in the electrode resistance to 0.16 Ωcm^2 at 1.8 $mgcm^{-2}$ (12.4 wt% $BaCO_3$). Therefore, there is an optimum loading weight for the infiltration phase related to the porosity of cathode frame, infiltration phase surface coverage in frame and other microstructural factors [47,48]. In this work, the LSCF electrode infiltrated with 1.2 $mgcm^{-2}$ (9.4 wt% $BaCO_3$), of $BaCO_3$ displayed the best performance.

Fig. 4b compares the stability of spray coated LSCF electrodes fabricated from pure $Ba(Ac)_2$ solution and surfactant modified $Ba(Ac)_2$ solutions. The sample fabricated from pure $Ba(Ac)_2$ solution exhibited a degradation in electrochemical performance when held at 600 °C for 600 h. The interfacial polarization resistance increased from 1.5 Ωcm^2 to 1.54 Ωcm^2 after 300 h and further increased to 1.62 Ωcm^2 after 600 h. In contrast, the LSCF electrode fabricated from a surfactant modified $Ba(Ac)_2$ solution remained quite stable over the extended duration test. The interfacial polarization resistance at the beginning of the test was 1.2 Ωcm^2, which only slightly increased to 1.29 Ωcm^2 after 300 h, followed by a subsequent decrease to 1.21 Ωcm^2 after 600 h of testing.

The TEM determined structure and microstructure of the $BaCO_3$ infiltrated LSCF electrode after 600 h testing at 600 °C are displayed in Fig. 5. The LSCF and $BaCO_3$ nanoparticles were well crystallized, as shown by clear lattice fringes and selected area electron diffraction (SAED) patterns, with characteristic diffraction spots identified zone axis, suggesting that the $BaCO_3$ nanoparticle maintains a highly crystalline structure even after 600 h testing at 600 °C. The spray coating process and resulting microstructure enables $BaCO_3$ to form highly crystalline regions, intimately connected with the LSCF frame which is believed to help to ensure the long term stability of the $BaCO_3$ infiltrated LSCF electrode.

Full cell SOFC measurements

A commercial anode supported cell with $BaCO_3$-infiltrated cathode and a baseline (unmodified) cell were comparatively tested at the multi-cell testing system at 750 °C for 500 h. The Bode plots of the impedance spectra at 24 h operation are presented in Fig. 6. It is evident that the resistive processes associated with the intermediate frequency (1–200 Hz) were primarily affected by $BaCO_3$-infiltration. According to previous impedance studies for anode-supported cells [49,50], the intermediate frequency processes are associated with fuel concentration polarization at anode and oxygen surface exchange kinetics/bulk diffusion at cathode. As the hydrogen utilization condition determined by the fuel flow rate and operating current should be identical for both cells, it is

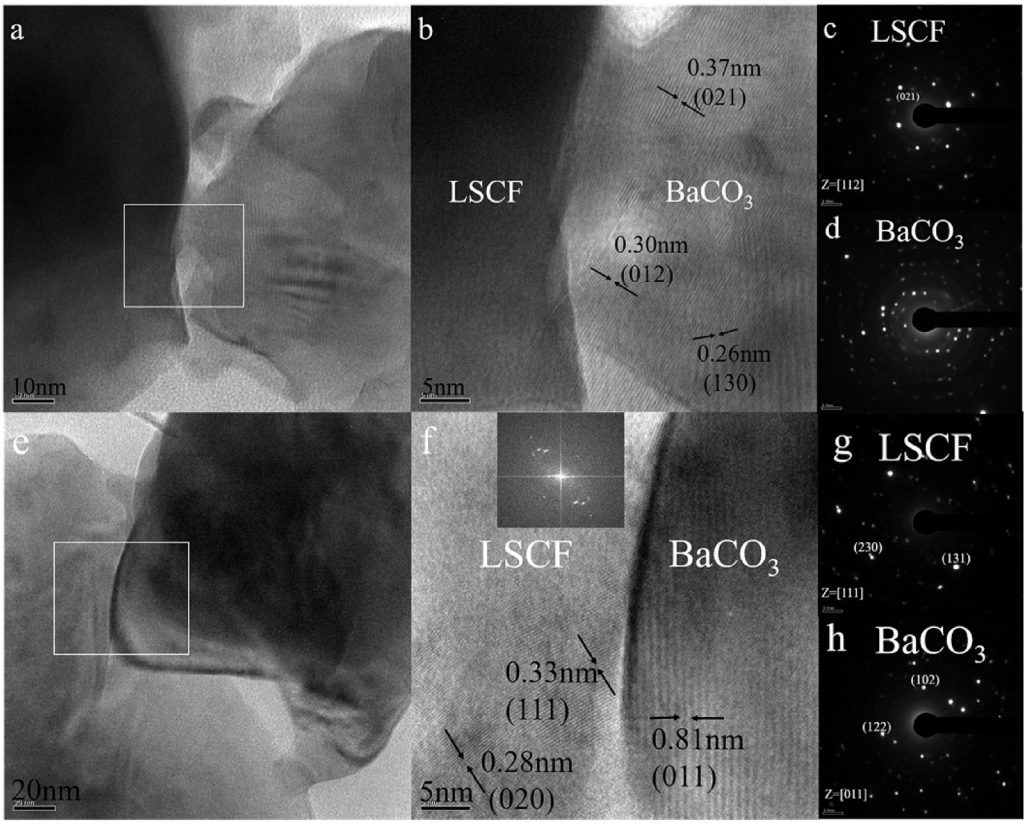

Fig. 5 – The TEM and SAED images for (a–d) modified $Ba(Ac)_2$ solution and (e–h) pure $Ba(Ac)_2$ solution spray coated LSCF electrode after 600 h long term stability test at 600 °C. The lattice parameter and indexed crystal structure for LSCF and $BaCO_3$ are also labeled.

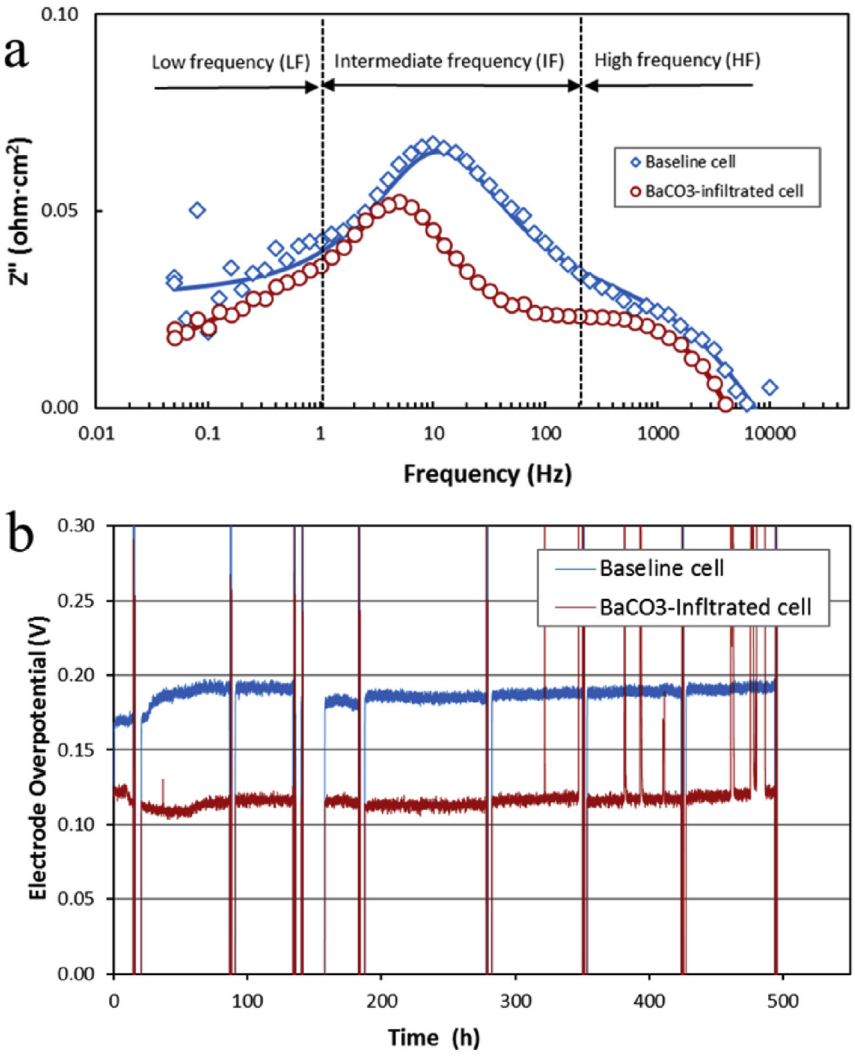

Fig. 6 – (a) Bode plot of the baseline cell and $BaCO_3$-infiltrated cell. The impedance spectra were measured under direct current density of 0.25 Acm^{-2} after 24 h operation at 750 °C. Solid lines are of simulated data fitted with the equivalent circuit model consisting of R_o, L, and two RQ elements. (b) Electrode overpotential variation with operation time of the baseline cell and $BaCO_3$-infiltrated cell, monitored under the current density of 0.25 Acm^{-2} at 750 °C. The electrode overpotential is derived by subtracting ohmic contribution from overall cell overpotential, which is the difference between Nernst potential (open circuit potential) and measured cell potential. The vertical lines in overpotential indicate the points when the cells were brought to open circuit condition for intermittent impedance measurements.

reasonably understood that the difference in the magnitude of the imaginary impedance is mainly related with the cathode activity. It is emphasized that the high frequency (>200 Hz) process that corresponds to the anode activation and the low frequency (<1 Hz) process of the cathode concentration polarization are not affected by the cathode infiltration, as expected.

Fig. 6b shows electrode overpotential variation of the baseline cell and the infiltrated cell at a constant current density of 0.25 Acm^{-2} for the operation of 500 h. It is apparent that electrode overpotential was significantly reduced by addition of $BaCO_3$ into the LSCF-SDC cathode. After the initial stabilization period (~180 h), both cells showed gradual increase in electrode overpotential. To identify the resistive processes that affect the temporal overpotential variation, impedance spectra measured at various operation time were fitted with an equivalent circuit composed of R_o, L and 2 RQ elements. These results are presented for the intermediate frequency (IF) processes and the high frequency (HF) processes in Fig. 7. For the baseline cell (Fig. 7a), the polarization resistance of the IF processes that includes the cathode activation polarization was higher than that of the HF processes which are primarily associated with the anode activation polarization (233 mV vs. 130 mV at 0 h). However, as shown in Fig. 7b, the infiltrated cell had a much reduced polarization resistance in the IF range (122 mV at 0 h) compared to the baseline cell and showed even lower resistance than that of the HF processes. While the polarization

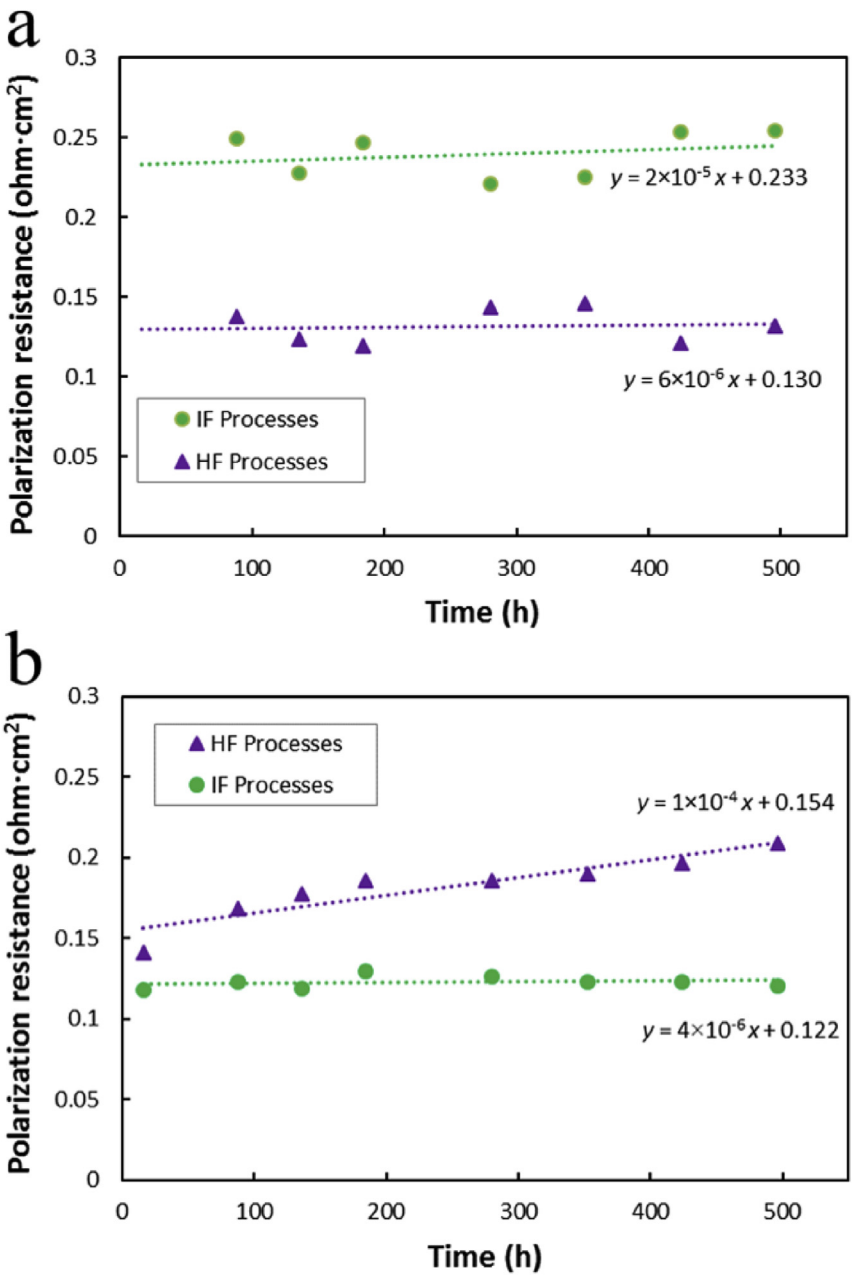

Fig. 7 – Area specific polarization resistances variation with operation time of (a) baseline cell and (b) $BaCO_3$-infiltrated cell as a function of operation time. All impedance spectra were measured under direct current density of 0.25 Acm^{-2}. Linear fitting data are shown as dotted lines with equations. The polarization resistances of high frequency (HF) processes and intermediate frequency (IF) processes were determined by fitting the impedance data to the equivalent circuit model consisting of R_o, L, and two RQ elements.

impedance originated from the anode (HF) increased by 25% for the infiltrated cell over the entire operation for 500 h, the resistance related with cathode (IF) was only changed by 1.6%. This implies that the activated cathode performance induced by the nanosized $BaCO_3$ electrocatalysts was maintained with high stability over the entire duration of cell operation.

The morphology of the $BaCO_3$ infiltrated cell after the 500 h long term test is shown in Fig. 8 demonstrating the LSCF-SDC cathode frame maintained its porous structure. After testing, the $BaCO_3$ nanoparticles were found to be isolated (not coarsened or agglomerated) on the LSCF-SDC backbone which is consistent with the excellent full cell long term stability and suggesting good catalytic activity [2,51]. The particle size observed after testing was 80 nm as confirmed in TEM image, which is indistinguishable from the particle size before testing. The unchanged microstructures also suggest stable electrochemical performance as discussed.

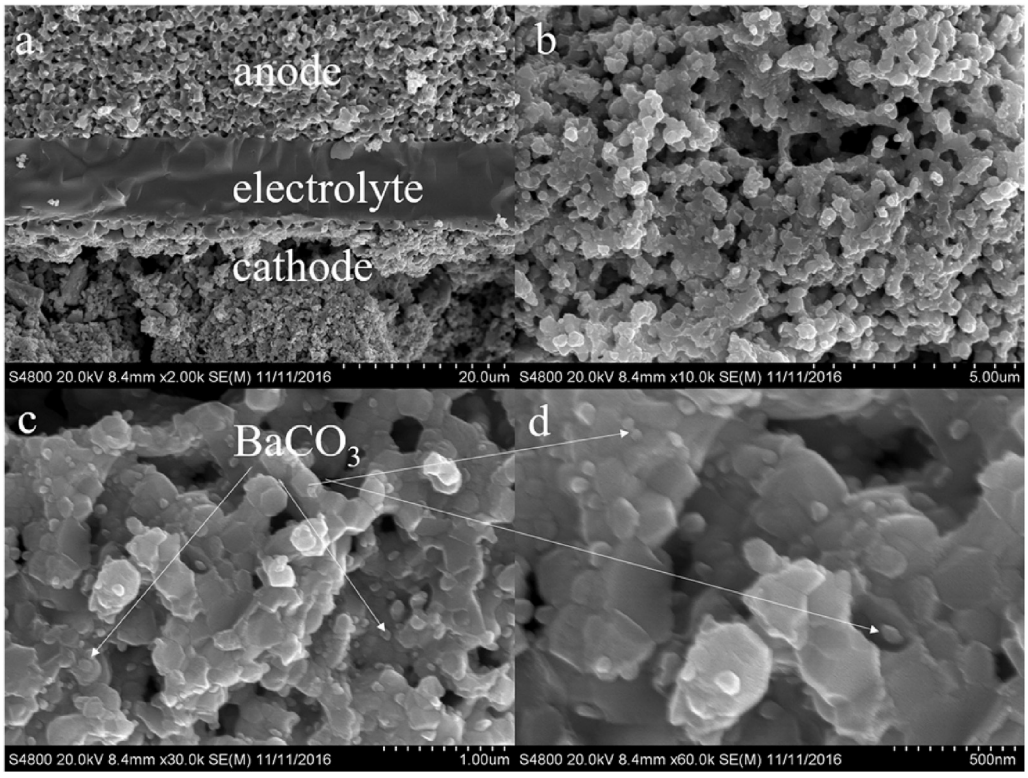

Fig. 8 – SEM images for MSRI full cell after 500 h discharge long term test. (a) Cross section image for whole cell, (b) LSCF-SDC cathode backbone that infiltrated with $BaCO_3$ and (c–d) enlarged area for cathode that isolated coated with $BaCO_3$ nanoparticles.

Conclusion

$BaCO_3$ nanoparticles were deposited on LSCF and commercial LSCF-SDC electrodes by a spray coating method. Solutions were modified with surfactant resulted in lower barium acetate decomposition temperature, reduced solution surface tension and decreased contact angle when deposited on LSCF scaffolds. After infiltration by spray coating, the $BaCO_3$ nanoparticles exhibited enhanced interfacial bonding with LSCF and fully penetrated the cathode area to the electrode/electrolyte interface. Spray coating infiltration of electrodes resulted in significant reduction in the polarization resistance. In addition to symmetrical cells, commercial full cell SOFCs also exhibited enhanced performance with $BaCO_3$ additions. After 500 h long term test at 750 °C, the electrode overpotential of spray infiltrated cells was observed to much lower than that of baseline cells. The polarization resistance of $BaCO_3$ infiltrated LSCF-SDC electrode only increased by 1.6% after 500 h testing at 750 °C demonstrating excellent stability. This work demonstrated a highly scalable spray coating process of a promising electrocatalyst ($BaCO_3$) with excellent long-term stability for the oxygen reduction reaction.

Acknowledgements

We gratefully acknowledge the financial support from the Department of Energy, Nuclear Energy Research Program (DOE-NEUP) Project 14-6357, A New Paradigm for Understanding Multi-phase Ceramic Waste Form Performance. KSB was supported in part by an appointment to the National Energy Technology Laboratory Research Participation Program, sponsored by the U.S. Department of Energy and administered by the Oak Ridge Institute for Science and Education.

REFERENCES

[1] Park S, Vohs JM, Gorte RJ. Direct oxidation of hydrocarbons in a solid-oxide fuel cell. Nature 2000;404:265–7.
[2] Rahimnejad M, Ghoreyshi AA, Najafpour GD, Younesi H, Shakeri M. A novel microbial fuel cell stack for continuous production of clean energy. Int J Hydrogen Energy 2012;37:5992–6000.
[3] Rahimnejad M, Najafpour GD, Ghoreyshi AA, Shakeri M, Zare H. Methylene blue as electron promoters in microbial fuel cell. Int J Hydrogen Energy 2011;36:13335–41.
[4] Babu VJ, Kumar MK, Nair AS, Kheng TL, Allakhverdiev SI, Ramakrishna S. Visible light photocatalytic water splitting for hydrogen production from $NTiO_2$ rice grain shaped electrospun nanostructures. Int J Hydrogen Energy 2012;37:8897–904.
[5] Zhang X, Liu L, Zhao Z, Tu B, Ou D, Cui D, et al. Enhanced oxygen reduction activity and solid oxide fuel cell performance with a nanoparticles-loaded cathode. Nano Lett 2015;15:1703–9.
[6] Lee JG, Park JH, Shul YG. Tailoring gadolinium-doped ceria-based solid oxide fuel cells to achieve 2 Wcm^{-2} at 550° C. Nat Commun 2014;5:4045.

[7] Sundarrajan S, Allakhverdiev SI, Ramakrishna S. Progress and perspectives in micro direct methanol fuel cell. Int J Hydrogen Energy 2012;37:8765–86.

[8] An J, Kim YB, Park J, Gür TM, Prinz FB. Three-dimensional nanostructured bilayer solid oxide fuel cell with 1.3 W/cm^2 at 450 °C. Nano Lett 2013;13:4551–5.

[9] Liang F, Zhou W, Chi B, Pu J, Jiang S, Li J. Pd-YSZ composite cathodes for oxygen reduction reaction of intermediate-temperature solid oxide fuel cells. Int J Hydrogen Energy 2011;36:7670–6.

[10] Hong T, Zhao M, Brinkman K, Chen F, Xia C. Enhanced oxygen reduction activity on Ruddlesden-Popper phase decorated $La_{0.8}Sr_{0.2}FeO_{3-\delta}$ 3D heterostructured cathode for solid oxide fuel cells. ACS Appl Mater Interfaces 2017;9:8659.

[11] Ding D, Liu M, Liu Z, Li X, Blinn K, Zhu X, et al. Efficient electro-catalysts for enhancing surface activity and stability of SOFC cathodes. Adv Energy Mater 2013;3:1149–54.

[12] Ding D, Li X, Lai SY, Gerdes K, Liu M. Enhancing SOFC cathode performance by surface modification through infiltration. Energy Environ Sci 2014;7:552–75.

[13] Jiang SP. Nanoscale and nano-structured electrodes of solid oxide fuel cells by infiltration: advances and challenges. Int J hydrogen energy 2012;37:449–70.

[14] Jiang Z, Xia C, Chen F. Nano-structured composite cathodes for intermediate-temperature solid oxide fuel cells via an infiltration/impregnation technique. Electrochim Acta 2010;55:3595–605.

[15] Park YM, Kim JH, Kim H. High-performance composite cathodes for solid oxide fuel cells. Int J Hydrogen Energy 2011;36:9169–79.

[16] Jiang Z, Lei Z, Ding B, Xia C, Zhao F, Chen F. Electrochemical characteristics of solid oxide fuel cell cathodes prepared by infiltrating (La, Sr) MnO_3 nanoparticles into yttria-stabilized bismuth oxide backbones. Int J Hydrogen Energy 2010;35:8322–30.

[17] Ni M, Leung M, Leung D. Technological development of hydrogen production by solid oxide electrolyzer cell (SOEC). Int J Hydrog Energy 2008;33:2337–54.

[18] Yang C, Jin C, Coffin A, Chen F. Characterization of infiltrated $(La_{0.75}Sr_{0.25})_{0.95}MnO_3$ as oxygen electrode for solid oxide electrolysis cells. Int J Hydrogen Energy 2010;35:5187–93.

[19] Van Dillen AJ, Terörde RJ, Lensveld DJ, Geus JW, De Jong KP. Synthesis of supported catalysts by impregnation and drying using aqueous chelated metal complexes. J Catal 2003;216:257–64.

[20] Galarraga C, Peluso E, De Lasa H. Eggshell catalysts for Fischer–Tropsch synthesis: modeling catalyst impregnation. Chem Eng J 2001;82:13–20.

[21] Murray EP, Sever M, Barnett S. Electrochemical performance of (La, Sr)(Co, Fe)O_3–(Ce, Gd)O_2 composite cathodes. Solid State Ionics 2002;148:27–34.

[22] Mai A, Haanappel VA, Uhlenbruck S, Tietz F, Stöver D. Ferrite-based perovskites as cathode materials for anode-supported solid oxide fuel cells: Part I. Variation of composition. Solid State Ionics 2005;176:1341–50.

[23] Waller D, Lane J, Kilner J, Steele B. The effect of thermal treatment on the resistance of LSCF electrodes on gadolinia doped ceria electrolytes. Solid State Ionics 1996;86:767–72.

[24] Chen J, Liang F, Chi B, Pu J, Jiang SP, Jian L. Palladium and ceria infiltrated $La_{0.8}Sr_{0.2}Co_{0.5}Fe_{0.5}O_{3-\delta}$ cathodes of solid oxide fuel cells. J Power Sources 2009;194:275–80.

[25] Lynch ME, Yang L, Qin W, Choi J-J, Liu M, Blinn K, et al. Enhancement of $La_{0.6}Sr_{0.4}Co_{0.2}Fe_{0.8}O_{3-\delta}$ durability and surface electrocatalytic activity by $La_{0.85}Sr_{0.15}MnO_{3\pm\delta}$ investigated using a new test electrode platform. Energy Environ Sci 2011;4:2249–58.

[26] Hong T, Chen F, Xia C. Barium carbonate nanoparticle to enhance oxygen reduction activity of strontium doped lanthanum ferrite for solid oxide fuel cell. J Power Sources 2015;278:741–50.

[27] Hong T, Brinkman KS, Xia C. Barium carbonate nanoparticles as synergistic catalysts for the oxygen reduction reaction on $La_{0.6}Sr_{0.4}Co_{0.2}Fe_{0.8}O_{3-\delta}$ solid-oxide fuel cell cathodes. ChemElectroChem 2016;3:805–13.

[28] Hong T, Chen F, Xia C. Barium carbonate nanoparticle as high temperature oxygen reduction catalyst for solid oxide fuel cell. Electrochem Commun 2015;51:93–7.

[29] Li M, Sun Z, Yang W, Hong T, Zhu Z, Zhang Y, et al. Mechanism for the enhanced oxygen reduction reaction of $La_{0.6}Sr_{0.4}Co_{0.2}Fe_{0.8}O_{3-\delta}$ by strontium carbonate. Phys Chem Chem Phys 2017;19:503–9.

[30] Bidrawn F, Kim G, Aramrueang N, Vohs J, Gorte R. Dopants to enhance SOFC cathodes based on Sr-doped $LaFeO_3$ and $LaMnO_3$. J Power Sources 2010;195:720–8.

[31] Li M, Zheng M, Hu B, Zhang Y, Xia C. Improving electrochemical performance of lanthanum strontium ferrite by decorating instead of doping cobaltite. Electrochim Acta 2017;230:196–203.

[32] Yamahara K, Jacobson CP, Visco SJ, Zhang X-F, De Jonghe LC. Thin film SOFCs with cobalt-infiltrated cathodes. Solid State Ionics 2005;176:275–9.

[33] Traulsen ML, McIntyre MD, Norrman K, Sanna S, Mogensen MB, Walker RA. Reversible decomposition of secondary phases in BaO infiltrated LSM electrodes—polarization effects. Adv Mater Interfaces 2016;3.

[34] Kim EH, Jung HJ, An KS, Park JY, Lee J, Hwang ID, et al. Degradation of $La_{0.6}Sr_{0.4}CoO_3$-based cathode performance in solid oxide fuel cells due to the presence of aluminum oxide deposited through atomic layer deposition. Ceram Int 2014;40:7817–22.

[35] Ai N, Chen K, Jiang SP, Lü Z, Su W. Vacuum-assisted electroless copper plating on Ni/(Sm, Ce)O_2 anodes for intermediate temperature solid oxide fuel cells. Int J Hydrogen Energy 2011;36:7661–9.

[36] Jung SW, Vohs JM, Gorte RJ. Preparation of SOFC anodes by electrodeposition. J Electrochem Soc 2007;154:B1270–5.

[37] Dowd RP, Lee S, Fan Y, Gerdes K. Engineering the solid oxide fuel cell electrocatalyst infiltration technique for industrial use. Int J Hydrogen Energy 2016;41:14971–81.

[38] Lu C, Sholklapper TZ, Jacobson CP, Visco SJ, De Jonghe LC. LSM-YSZ cathodes with reaction-infiltrated nanoparticles. J Electrochem Soc 2006;153:A1115–9.

[39] Sholklapper TZ, Lu C, Jacobson CP, Visco SJ, De Jonghe LC. LSM-infiltrated solid oxide fuel cell cathodes. Electrochem Solid-State Lett 2006;9:A376–8.

[40] Zhu W, Ding D, Xia C. Enhancement in three-phase boundary of SOFC electrodes by an ion impregnation method: a modeling comparison. Electrochem Solid-State Lett 2008;11:B83–6.

[41] Nicholas JD, Barnett SA. Finite-element modeling of idealized infiltrated composite solid oxide fuel cell cathodes. J Electrochem Soc 2009;156:B458–64.

[42] Shah M, Nicholas JD, Barnett SA. Prediction of infiltrated solid oxide fuel cell cathode polarization resistance. Electrochem Commun 2009;11:2–5.

[43] Bidrawn F, Küngas R, Vohs JM, Gorte RJ. Modeling impedance response of SOFC cathodes prepared by infiltration. J Electrochem Soc 2011;158:B514–25.

[44] Zhang Y, Xia C. A durability model for solid oxide fuel cell electrodes in thermal cycle processes. J Power Sources 2010;195:6611–8.

[45] Nie L, Liu M, Zhang Y, Liu M. $La_{0.6}Sr_{0.4}Co_{0.2}Fe_{0.8}O_{3-\delta}$ cathodes infiltrated with samarium-doped cerium oxide for solid oxide fuel cells. J Power Sources 2010;195:4704–8.
[46] Sahibzada M, Benson S, Rudkin R, Kilner J. Pd-promoted $La_{0.6}Sr_{0.4}Co_{0.2}Fe_{0.8}O_{3-\delta}$ cathodes. Solid State Ionics 1998;113:285–90.
[47] Zhang Y, Sun Q, Xia C, Ni M. Geometric properties of nanostructured solid oxide fuel cell electrodes. J Electrochem Soc 2013;160:F278–89.
[48] Zhang Y, Ni M, Xia C. Microstructural insights into dual-phase infiltrated solid oxide fuel cell electrodes. J Electrochem Soc 2013;160:F834–9.
[49] Endler C, Leonide A, Weber A, Tietz F, Ivers-Tiffée E. Time-dependent electrode performance changes in intermediate temperature solid oxide fuel cells. J Electrochem Soc 2010;157:B292–8.
[50] Lee S, Miller N, Gerdes K. Long-term stability of SOFC composite cathode activated by electrocatalyst infiltration. J Electrochem Soc 2012;159:F301–8.
[51] Gao Z, Mogni LV, Miller EC, Railsback JG, Barnett SA. A perspective on low-temperature solid oxide fuel cells. Energy Environ Sci 2016;9:1602–44.